frontiers | Frontiers in Physics

TYPE Original Research
PUBLISHED 30 July 2024
DOI 10.3389/fphy.2024.1401834

OPEN ACCESS

EDITED BY
Angeles Faus Golfe,
UMR9012 Laboratoire de Physique des 2 infinis Irène Joliot-Curie (IJCLab), France

REVIEWED BY
Lanchun Lu,
The Ohio State University, United States
Claus Andersen,
Technical University of Denmark, Denmark
Itzhak Orion,
Ben-Gurion University of the Negev, Israel

*CORRESPONDENCE
James Cayley,
jcayley@uow.edu.au

RECEIVED 16 March 2024
ACCEPTED 04 July 2024
PUBLISHED 30 July 2024

CITATION
Cayley J, Tan Y-RE, Petasecca M, Cutajar D, Breslin T, Rosenfeld A and Lerch M (2024), MOS*kin* dosimetry for an ultra-high dose-rate, very high-energy electron irradiation environment at PEER.
Front. Phys. 12:1401834.
doi: 10.3389/fphy.2024.1401834

MOS*kin* dosimetry for an ultra-high dose-rate, very high-energy electron irradiation environment at PEER

James Cayley[1]*, Yaw-Ren E. Tan[2], Marco Petasecca[1], Dean Cutajar[1], Thomas Breslin[3], Anatoly Rosenfeld[1] and Michael Lerch[1]

[1]Centre for Medical Radiation Physics, University of Wollongong, Wollongong, NSW, Australia, [2]Australian Synchrotron, ANSTO, Melbourne, VIC, Australia, [3]Department of Oncology, Clinical Sciences, Lund University, Lund, Sweden

FLASH radiotherapy, which refers to the delivery of radiation at ultra-high dose-rates (UHDRs), has been demonstrated with various forms of radiation and is the subject of intense research and development recently, including the use of very high-energy electrons (VHEEs) to treat deep-seated tumors. Delivering FLASH radiotherapy in a clinical setting is expected to place high demands on real-time quality assurance and dosimetry systems. Furthermore, very high-energy electron research currently requires the transformation of existing non-medical accelerators into radiotherapy research environments. Accurate dosimetry is crucial for any such transformation. In this article, we assess the response of the MOS*kin*, developed by the Center for Medical Radiation Physics, which is designed for on-patient, real-time skin dose measurements during radiotherapy, and whether it exhibits dose-rate independence when exposed to 100 MeV electron beams at the Pulsed Energetic Electrons for Research (PEER) end-station. PEER utilizes the electron beam from a 100 MeV linear accelerator when it is not used as the injector for the ANSTO Australian Synchrotron. With the estimated pulse dose-rates ranging from $(7.84 \pm 0.21) \times 10^5$ Gy/s to $(1.28 \pm 0.03) \times 10^7$ Gy/s and an estimated peak bunch dose-rate of $(2.55 \pm 0.06) \times 10^8$ Gy/s, MOS*kin* measurements were verified against a scintillating screen to confirm that the MOS*kin* responds proportionally to the charge delivered and, therefore, exhibits dose-rate independence in this irradiation environment.

KEYWORDS

skin dose, FLASH, dosimetry, very high-energy electrons, MOS*kin*, ultra-high dose-rate, VHEE

1 Introduction

FLASH radiotherapy is an emerging cancer treatment modality that utilises much higher dose-rates than conventional radiotherapy. Recent evidence published indicates that delivering radiation with ultra-high dose-rates (UHDRs) results in a so-called "FLASH effect," whereby healthy tissue is spared and the effects on normal bodily function are reduced while maintaining adequate tumor control [1–5]. The FLASH effect has been demonstrated at average treatment dose-rates ($\dot{D}_t$) above 40 Gy/s (gray; 1 Gy = 1 J/kg) for

various radiation types, including x-rays, protons, and electrons [6, 7]. The use of very high-energy electrons (VHEEs) (above 50 MeV) has been considered for the treatment of deep-seated tumors [8, 9].

Converted medical linear accelerators (linacs) are being used to deliver UHDR electrons. To provide the required dose-rates, the conversion often requires the removal or modification of transmission ion chambers in the head of the linac [10–12] that are used for beam interruption if the radiation delivery diverges from the treatment plan. In the absence of traditional beam interruption systems, there have been advances in fluence monitoring using beam current transformers and pulse delivery optimization systems [13–15]. However, while such advances have been successful and are very important tools for monitoring the delivery of radiation by the linac, these are not forms of dosimetry and so should not be used in isolation for quality assurance. Malfunctioning or mispositioned linac components, such as the jaws or multi-leaf-collimator, installed after the target will cause changes in the dose that are not reflected in the linac beam current.

A critical metric for any external beam radiotherapy modality is the true dose delivered to the patient, often inferred from *in vivo* dosimetry by measuring the dose to the skin, which is itself an important metric [16, 17]. Radiotherapy, of differing types and energies, delivers a dose to the patient's skin that may be high or low relative to the point of maximum dose. When discussing skin dose, the region of interest is the radio-sensitive basal cell layer that resides at the inner-most end of the epidermis at an average depth of 70 μm [16–18]. Although future VHEE treatments may deliver a low skin dose relative to the maximum dose [19–21], the dose should be quantified via *in vivo* measurements and can be used for quality assurance during patient treatment. Current UHDR dosimetry mostly relies upon GafChromic film [11, 22, 23], although other forms of dosimetry such as calorimeters and modified ionization chambers have also been successfully demonstrated as suitable [24, 25]. However, these forms of dosimetry either require complicated setups, lack the near real-time results highly desired in a clinical setting, or are not suitable for evaluating skin dose during treatment delivery. Metal oxide semiconductor field effect transistor (MOSFET) dosimeters offer a promising solution for UHDR environments, which are known for their dose-rates independence, having previously been tested using an electron linac with dose-rates up to 10^7 Gy/s [26]. The Center for Medical Radiation Physics developed MOS*kin* features a design, construction, and packaging distinct from traditional MOSFETs, making them more suitable for clinical dosimetry, especially for the skin [27–29]. With a silicon die approximately 0.168 mm^3 in volume, beam perturbation is negligible at megavoltage and kilovoltage energies [30–33], allowing the device to be attached to the patient for real-time quality assurance during treatment. The sensitive volume is only 0.55 μm thick and can be manufactured in a wide range, from a few micrometers to a few nanometers. Thickness is used to control the sensitivity of the device to ionizing radiation [34, 35]. The MOS*kin* has been validated for on-patient quality assurance skin dose measurements during conventional radiotherapy treatments using x-rays or electrons, where it exhibits a linear response up to 50 Gy [36]. Importantly, for potential UHDR VHEE environments, the MOS*kin* exhibited dose-rate independence in previous studies for clinical use at lower electron energies ranging from 4 MeV to 20 MeV [37, 38], where dose-rates are orders of magnitude lower for medical linacs [39].

Modern medical linacs deliver pulsed electron beams that consist of a sub-structure of electron bunches [40, 41]. Therefore, when discussing dose-rates for medical purposes, not only $\dot{D}_t$ is important, but also the dose-per-pulse (DPP) and dose-per-bunch (DPB) may impact the UHDR radiotherapy effectiveness. DPP and DPB are also expected to impact the response of detectors used for dosimetry. For some commercial detectors, the DPP becomes a limiting factor as it increases above 10 cGy [42]. To increase the DPP, ultra-high pulse dose-rates ($\dot{D}_p$, the dose within the pulse divided by the temporal length of the pulse) are required. As bunches have a non-zero temporal component, the bunch dose-rate ($\dot{D}_b$, the dose within a single bunch, divided by the temporal length of the bunch) must also be considered as it can be multiple orders of magnitude higher than $\dot{D}_t$ and $\dot{D}_p$ and will be "experienced" by a detector as charge generation will occur over these timescales. As medical linacs cannot provide VHEE and are limited in the adjustment of parameters, we take advantage of the new Pulsed Energetic Electrons for Research (PEER), at the heart of which is a custom-built research linac, which has recently become available to selected users when it is not being used as the injector at the ANSTO Australian Synchrotron (AS). The PEER linac accelerates electrons to 100 MeV, in pulses with $\dot{D}_p$ as high as 10^7 Gy/s. As the only linac of its kind available for research in Australia, ongoing transformation to dual-use for synchrotron injection and research will provide previously unavailable capabilities and inform the design choices of future facilities catering to user needs. Dosimetry studies are crucial to characterizing PEER for ongoing medical and VHEE research. In this work, we demonstrate that dose-rate independence exists when the MOS*kin* is exposed to the VHEE beam at PEER.

2 Materials and methods

For an in-depth discussion of the general construction and operation of MOSFET detectors, please refer to [43]. The MOS*kin*s are exposed to the VHEE irradiation field, creating electron–hole pairs in the gate oxide (SiO_2). The gate oxide is biased during irradiation, causing electrons to drift toward the gate electrode, where they are collected. Furthermore, the holes drift toward the substrate and are trapped at the Si/SiO_2 interface defect centers created during the MOS*kin* production process. However, unlike ionization chambers and other solid-state detectors, ionization current is not the response of interest. Instead, the effect of radiation damage via the accumulation of trapped holes causes a quantifiable change in the operating parameters of the device, allowing the dose to be measured. In these p-channel MOS*kin*s, the trapped holes decrease the local hole space-charge density in the p-channel via Coulomb repulsion. This decreased density effectively increases the resistivity of the source-drain p-channel, increasing the measured gate threshold voltage (V_{th}) for a desired source-drain current. The change in V_{th} per unit of the absorbed irradiation dose in the gate oxide is highly reproducible and is also a measure of the sensitivity of the MOS*kin* to the exposing irradiation field environment [43]. Used as a relative dosimeter, the

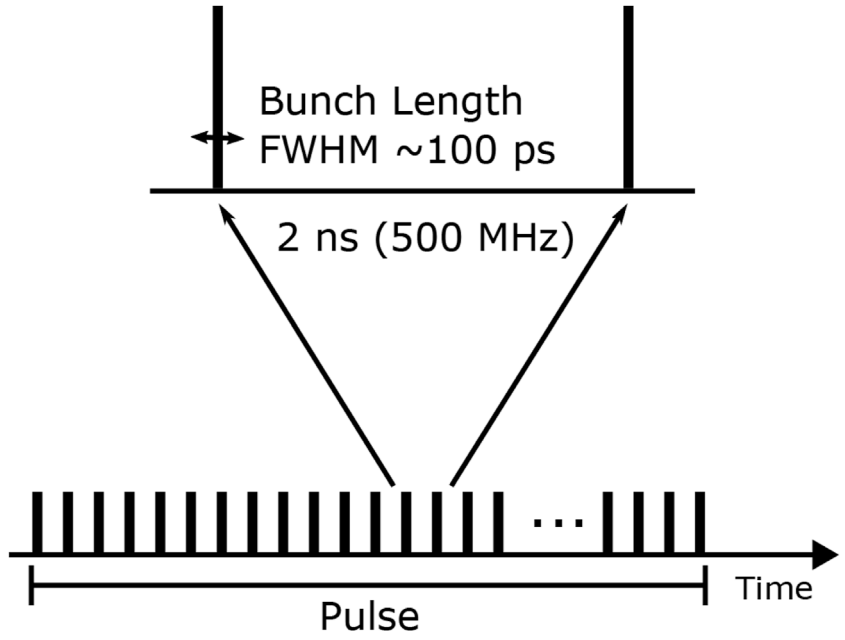

FIGURE 1
Electron linac pulses consist of an underlying bunch structure. PEER parameters are shown.

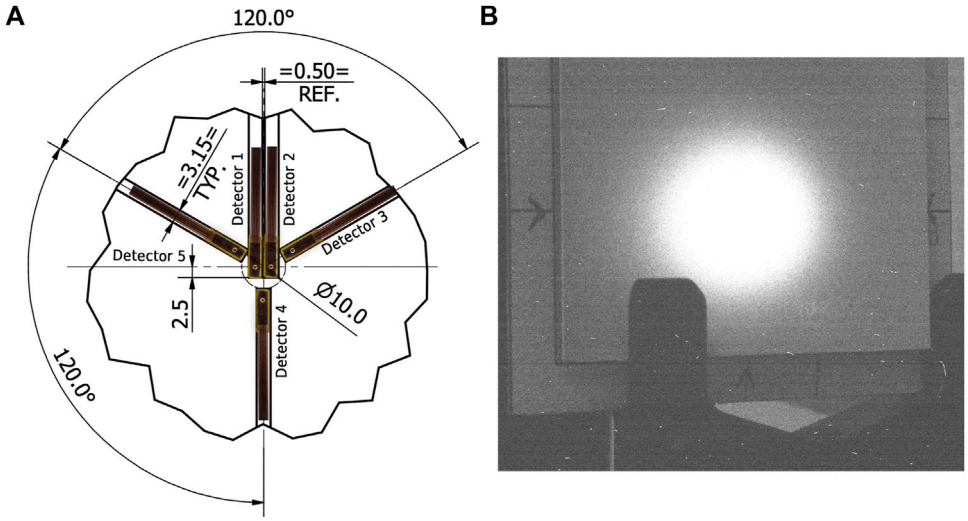

FIGURE 2
(A) Array design with MOS*kin*s overlaid for clarity. Unless otherwise stated, dimensions are in mm. **(B)** Camera image showing scintillating screen with arrows indicating the center of array alignment.

sensitivity is ΔV_{th} / 1 cGy and is used to convert the measured change in V_{th} to the absorbed dose [44].

The VHEE beam at PEER features a custom-built research linac, which is normally used to inject bunched 100 MeV electrons into the AS. The linac is capable of delivering pulses with expected $\dot{D}_p$ of 10^7 Gy/s on nanosecond timescales, and as displayed in Figure 1, it operates with an intra-bunch frequency of 500 MHz and a bunch length of approximately 100 ps. Like medical linacs, a sequence of bunches forms a single pulse [45]. Pulses are delivered at a pulse repetition frequency of 1 Hz (up to 10 Hz will be available in the very near future), with pulse duration ranging from 16 ns to 1000 ns. Electrons exit the linac into air through a 125 μm titanium foil window with a transverse bunch size (sigma) of 1.2 mm in *x* and *y* directions. A fast current transformer (FCT) is used to measure the beam current. As the linac is still undergoing a transformation into a facility for select, by-appointment beamtime, its wide range of capabilities may be restricted to a smaller sub-set where modifications to standard operating conditions are needed.

Two MOS*kin* detectors (Detectors 1 and 2 shown in Figure 2A) were mounted on a 6 mm polymethyl methacrylate frame, positioned on the horizontal axis to measure the dose at the center of the beam. Furthermore, three MOS*kin*s (Detectors 3, 4, and 5 shown in Figure 2A) were positioned around the central axis to detect any undesired beam movement. Any change in the lateral 2D distribution of the beam intensity would be measured as a change in the point dose by the MOS*kin*s. The array was aligned with the VHEE beam using a laser. As an independent measure of beam intensity distribution change, a scintillating screen was positioned behind the MOS*kin*s and imaged using a Mako G-158B PoE camera. These images cannot provide an estimate of the dose, although this technique can be used to verify the relative consistency of fluence between pulses. Although the use of film would appear to be appropriate, with PEER in the early stages of its transformation into a usable research beam, operational and access requirements at the AS facility render it logistically impractical as currently the time required to change film between pulses is in the order of 25–30 minutes.

During the timeframe in which the following experiment was conducted, pulses consisting of 0.300 nC were available. This was a linac constraint at the time to ensure consistent charge per pulse while being able to vary the pulse length. Pulse lengths were on nanosecond timescales, enabling the ultra-high $\dot{D}_p$ necessary for eventual VHEE FLASH radiotherapy. In future experiments, higher DPP will be achieved by increasing the charge within each pulse, delivered over larger timescales. Consequently, $\dot{D}_p$ are expected to remain similar.

Before dosimetry commenced, the VHEE beam was aligned with the center of the scintillator using the arrows visible in Figure 2B, as this was aligned to the array of MOS*kin*s. After beam alignment, single 0.300 nC pulses were delivered across 13 VHEE beam currents, with a requested duration between 20 ns and 400 ns in length. Beam current and, therefore, pulse lengths were varied by adjusting the number of bunches within the pulse, with the intra-bunch spacing fixed at 2 ns. As a result, the charge in each bunch varied, leading to a modified DPB, although the bunch length remained fixed at 100 ps. This method ensured the total charge within a pulse and, therefore, DPP was constant, while $\dot{D}_p$ and $\dot{D}_b$ varied. To calculate the dose, V_{th} must be measured before and after exposure to radiation, and then, a calibration factor representing the sensitivity of the device to a given radiation source is applied to ΔV_{th}. Throughout the experiment, we used a standard MOS*kin* sensitivity of 2.53 ± 0.03mV/cGy, previously calibrated in clinical 6 MV x-ray environments [44], to estimate dose and dose-rates. Further investigation into MOS*kin* sensitivity within VHEE fields is, of course, required. However, this work investigates dose-rate independence, where a consistent response of the MOS*kin* across a range of dose-rates is important rather than absolute dose. To ensure consistency, a script was used to control both the delivery of linac pulses and read the MOS*kin* response before and after each pulse. With nine repeats for each beam current, we report an average with a 95% confidence interval of the MOS*kin* and scintillator responses.

3 Results

An average of $(0.305 +- 0.004)$ nC of charge was delivered in each pulse, as measured by the FCT. The responses of each detector once converted to dose revealed an estimated average DPP of (40.10 ± 0.52) cGy for Detector 1 and (29.32 ± 0.44) cGy for Detector 2, both higher than the 10 cGy limit causing saturation for many commercially available detectors. The responses of the remaining detectors were converted to dose, and then, all readings were normalized to the charge recorded by the FCT for each pulse. These results are shown in Figure 3 and are stable at beam currents above 2 mA, below which a sharp fall off occurs, which was not reflected in the FCT measurements. $\dot{D}_p$ for each pulse was estimated using Detector 1 measurements and range from approximately $(7.84 \pm 0.21) \times 10^5$ Gy/s to $(1.28 \pm 0.03) \times 10^7$ Gy/s, with a peak $\dot{D}_b$ of $(2.55 \pm 0.06) \times 10^8$ Gy/s. $\dot{D}_b$ is calculated as the dose measured within a pulse divided by the number of bunches within the pulse and then divided by the 100 ps temporal length of a bunch. Estimates of $\dot{D}_p$ and $\dot{D}_b$ for each beam current are shown in Table 1.

Using spatial information gained from the array, beam profiles were created from the scintillator data using ImageJ software [46] at the estimated vertical location of Detectors 1 and 2. Typically, a Gaussian distribution would be fitted to beam profiles; however, this was not a good fit for the PEER beam due to high dose gradients in the penumbra region. Instead, a Moffat distribution was used. The Moffat distribution is a modified Lorentzian distribution created to model point-source astronomical objects with steep fall-off gradients [47], which is defined as

$$A\left(1 + \frac{(x - x_0)^2}{\gamma^2}\right)^{-\alpha},$$

where A is the amplitude, x_0 is the center of the distribution, and γ and α are the fitting parameters. Figure 4 demonstrates the difference in beam profile and, therefore, charge delivery between high and low beam currents. The response of Detector 1 remained flat, indicating that its location was within the region of peak amplitude, where gradients are not as steep and the response will be less affected by beam movement. Hence, the value of the Moffat distribution was extracted at x_0, the estimated location of Detector 1.

To assess the behavior of Detector 2, the value was extracted at a fixed point 3.65 mm to the right of x_0 at the highest beam current due to the spacing between the sensitive volumes of detectors 1 and 2 on the array. This was repeated for each pulse to calculate the average response of the scintillator at the estimated locations of detectors 1 and 2 for each beam current. The experimental data used for the beam profiles contain spikes that lie outside the distribution; however, these are radiation-induced noise in the camera images. The results from the scintillator were normalized to 1, which enabled plotting against MOS*kin* data, also normalized to 1, to compare detector response against the charge delivered. Figure 5A displays this comparison for Detector 1, and the same trend is observed in both the MOS*kin* and scintillator responses. The same comparison is found in Figure 5B for Detector 2.

4 Discussion

Due to the design of the array (Figure 2A), the two central detectors should respond equally if the array were aligned perfectly to the beam, and the out-of-field detectors 3, 4, and 5 should also exhibit an equal response due to the Gaussian-like distribution of

10.3389/fphy.2024.1401834

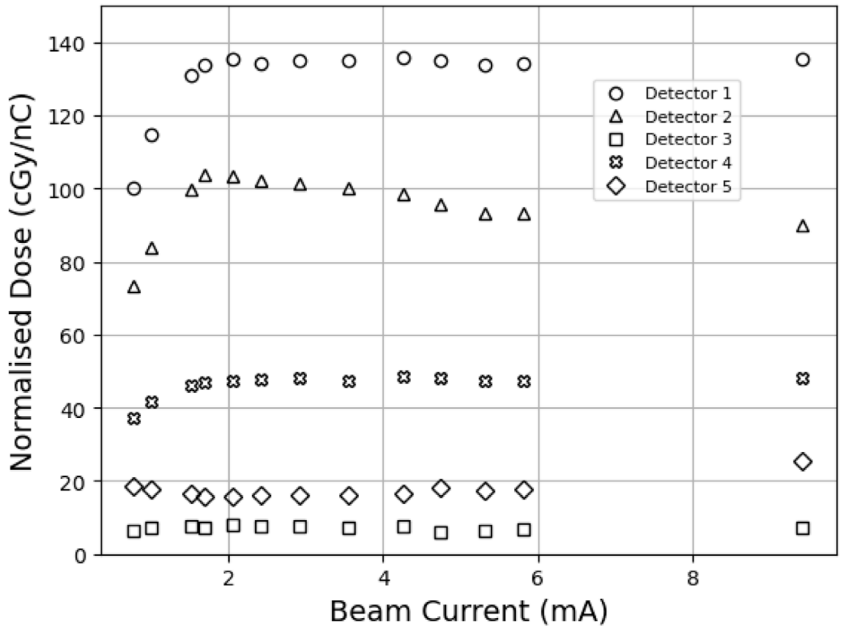

FIGURE 3
MOS*kin* responses converted to dose and normalized to charge as measured by FCT. A 95% confidence interval is within markers. Pulse lengths (nanosecond timescale) are inversely proportional to the beam current. The variation in MOS*kin* response across the symmetrical array allows the assessment of the beam position during the timeframe over which the experiment was conducted.

TABLE 1 Estimated mean $\dot{D}_p$ and $\dot{D}_b$. Bunches have a fixed temporal length of 100 ps. All values have a 95% confidence interval of ± 2.7% or less.

Pulse length (ns)	Detector 1 (Gy/s)		Detector 2 (Gy/s)	
	Pulse ($\times 10^6$)	Bunch ($\times 10^8$)	Pulse ($\times 10^6$)	Bunch ($\times 10^8$)
32	12.8	2.55	8.48	1.70
52	7.81	1.56	5.43	1.09
58	7.12	1.42	4.95	0.990
64	6.42	1.28	4.54	0.907
72	5.79	1.16	4.21	0.841
86	4.80	0.960	3.55	0.711
106	3.93	0.786	2.95	0.591
128	3.24	0.649	2.47	0.495
148	2.80	0.560	2.13	0.426
178	2.26	0.453	1.76	0.351
208	1.98	0.396	1.51	0.302
314	1.15	0.230	0.841	0.168
414	0.78	0.157	0.575	0.115

electron beams combined with the radial symmetry of the detector positioning on the array. The relative response between detectors, as shown in Figure 3, indicates a misalignment consistent with the position of the array relative to the central beam axis. This misalignment is also shown in Figure 2B, where the arrows marked on the scintillator reflect the vertical and horizontal positioning of the center of the array; the scintillator shows a response consistent with the findings from the relative MOS*kin* responses. Detector 5 responses decreased as the beam current decreased, in contrast to Detector 2, indicating that the beam also shifted horizontally throughout the experiment. Throughout the analysis, x_0, the center of the fitted Moffat distribution was found to shift to the right as the beam current decreased, supporting the indication that the center of the beam shifted as the experiment

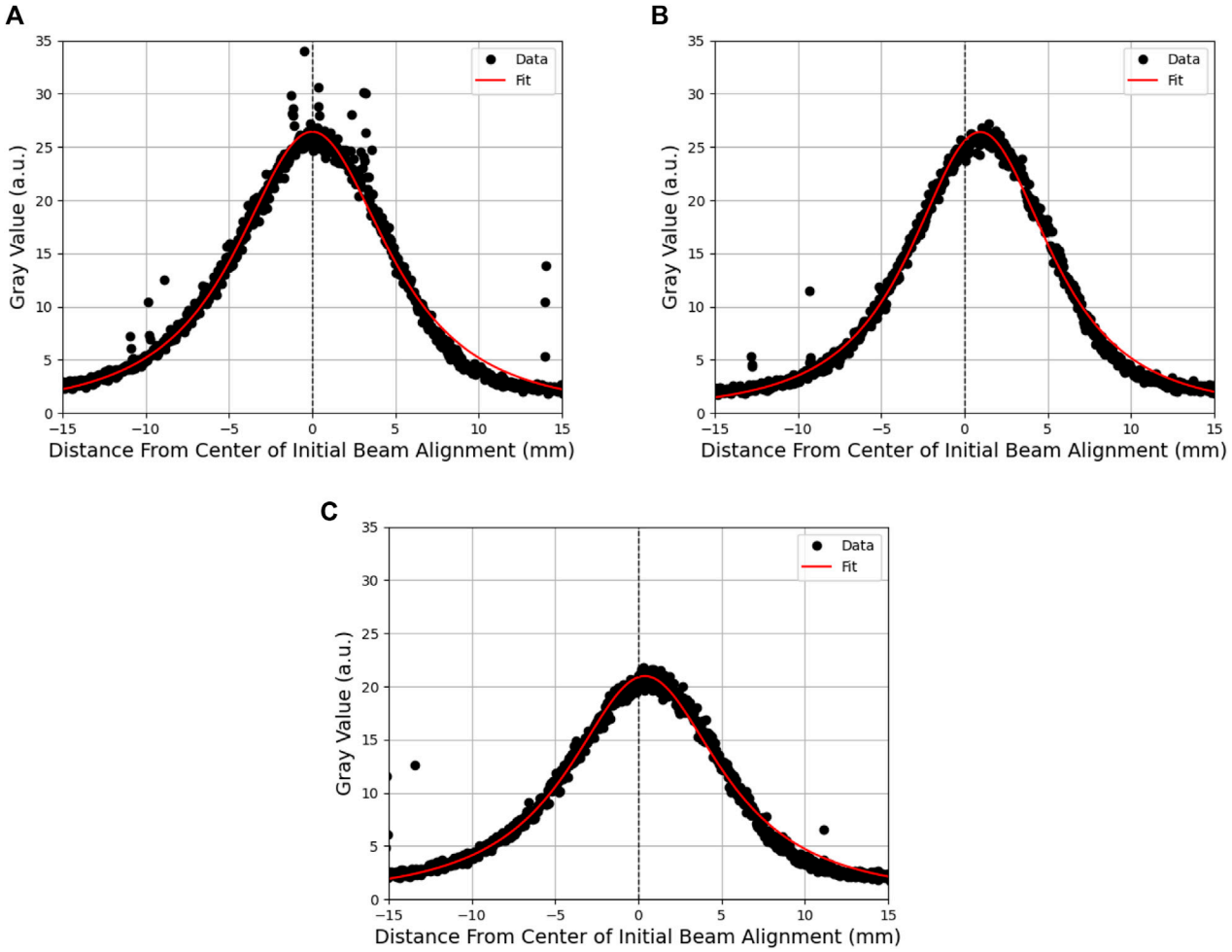

FIGURE 4
Moffat distribution fitted to scintillator beam profiles of a single pulse at a **(A)** high beam current, **(B)** the point at which detector response begins to fall off, and **(C)** low beam current. The difference in intensity between high and low beam currents is visible as a reduction in the magnitude of the profile and the movement of the beam from the initial alignment.

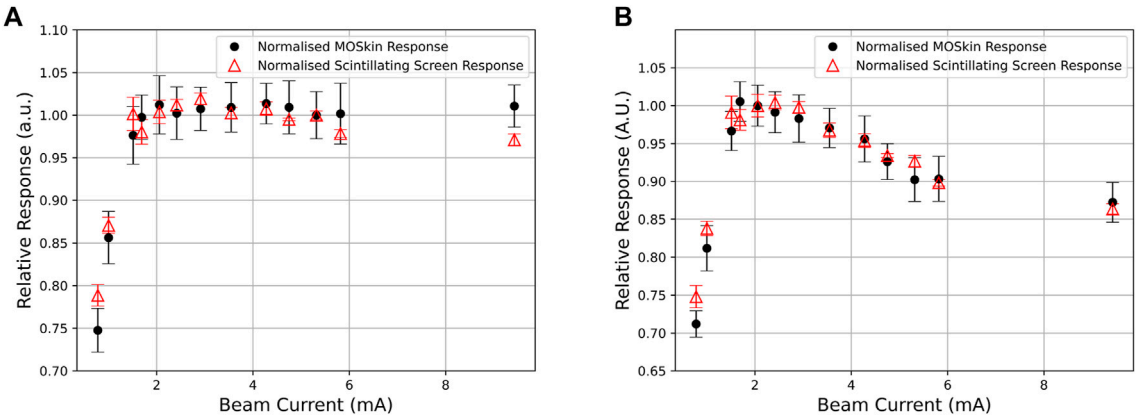

FIGURE 5
(A,B) Relative response of each pulse between the MOS*kin* and scintillating screen for Detector 1 and Detector 2, respectively.

moved from high to low beam current. Detector 2 was positioned 3.65 mm to the right of Detector 1, exposing it to the steep dose gradients, as evident in Figure 4, and, therefore, undesired beam movement caused a large change in the response of the detector at that point. This accounts for the increase in Detector 2 response throughout the experiment. When using the scintillator to verify the consistency of fluence between pulses, it is plausible that it has an intrinsic dependence on beam current/dose-rate. However, detectors 1 and 2 experienced different doses over the same timescales during the experiment and, hence, experienced different dose-rates. If the scintillator possessed a dose-rate dependence equivalent to that of a MOS*kin* detector, it would not be possible to correlate the responses of both detectors 1 and 2 with the scintillator response.

The observed fall-off in the MOS*kin* response below 2 mA indicates either an incorrect response from the MOS*kin*s or an error in charge delivery to the experimental stage. However, after analyzing the scintillator response and comparing the normalized data shown in Figure 5, it is clear that this fall-off is common to both instruments and must be due to a loss of charge from the linac rather than an incorrect reading from the MOS*kin*s. These results indicate that the MOS*kin* responds proportionally to the charge delivered to the experimental stage rather than changing beam current and thus exhibits dose-rate independence when exposed to the VHEE beam at PEER.

Of further importance is the discovery of the limitations of the FCT. Although the PEER FCT was originally commissioned to monitor beam currents during daily AS operation, this work provides important insight into the potential limitations of such devices. With efforts being made to correlate dose delivery to beam current transformers and other fluence monitoring devices on existing and new linacs for UHDR RT, these results suggest a requirement for accurate quality assurance dosimetry in conjunction with online monitoring devices as part of any future UHDR VHEE quality assurance.

5 Conclusion

While being exposed to $\dot{D}_p$ up to $(1.28 \pm 0.03) \times 10^7$ Gy/s, with $\dot{D}_b$ as high as $(2.55 \pm 0.06) \times 10^8$ Gy/s, the MOS*kin*s showed a response consistent with the scintillating screen, hence proportional to the charge delivered. This explains the observed trends in the MOS*kin* response and indicates dose-rate independence. FCT measurements were found to be an unreliable diagnostic for verifying dose delivery; however, this study instills confidence in the use of MOS*kin* for eventual UHDR VHEE quality assurance and skin dosimetry and justifies further work toward realization.

Data availability statement

The raw data supporting the conclusions of this article will be made available by the authors, without undue reservation.

Author contributions

JC: conceptualization, formal analysis, investigation, methodology, visualization, writing–original draft, and writing–review and editing. Y-RT: conceptualization, data curation, investigation, methodology, resources, software, supervision, and writing–review and editing. MP: conceptualization, investigation, methodology, and writing–review and editing. DC: conceptualization, investigation, methodology, and writing–review and editing. TB: conceptualization, investigation, methodology, and writing–review and editing. AR: conceptualization, funding acquisition, investigation, methodology, resources, supervision, and writing–review and editing. ML: conceptualization, funding acquisition, investigation, methodology, resources, supervision, and writing–review and editing.

Funding

The authors declare that financial support was received for the research, authorship, and/or publication of this article. JC received Australian Government RTP scholarship APP505948.

Acknowledgments

This research was undertaken on the PEER beamline, Australian Synchrotron, part of ANSTO. The authors would like to thank Khonraed Gill for the creation of engineering drawings and STEP files.

Conflict of interest

ML, AR, MP, and DC declare consulting with Electrogenics Laboratories Ltd., which is commercializing the MOSkin detector.

The remaining authors declare that the research was conducted in the absence of any commercial or financial relationships that could be construed as a potential conflict of interest.

The authors declared that they were an editorial board member of Frontiers, at the time of submission. This had no impact on the peer review process and the final decision.

Publisher's note

References

1. Favaudon V, Caplier L, Monceau V, Pouzoulet F, Sayarath M, Fouillade C, et al. Ultrahigh dose-rate FLASH irradiation increases the differential response between normal and tumor tissue in mice. *Sci Translational Med* (2014) 6:245ra93. doi:10.1126/scitranslmed.3008973

2. Montay-Gruel P, Acharya MM, Gonçalves Jorge P, Petit B, Petridis IG, Fuchs P, et al. Hypofractionated FLASH-RT as an effective treatment against glioblastoma that reduces neurocognitive side effects in mice. *Clin Cancer Res* (2021) 27:775–84. doi:10.1158/1078-0432.CCR-20-0894

3. Chabi S, To THV, Leavitt R, Poglio S, Jorge PG, Jaccard M, et al. Ultra-high-dose-rate FLASH and conventional-dose-rate irradiation differentially affect human acute lymphoblastic leukemia and normal hematopoiesis. *Int J Radiat Oncol - Biol - Phys* (2021) 109:819–29. doi:10.1016/j.ijrobp.2020.10.012

4. Simmons DA, Lartey FM, Schüler E, Rafat M, King G, Kim A, et al. Reduced cognitive deficits after FLASH irradiation of whole mouse brain are associated with less hippocampal dendritic spine loss and neuroinflammation. *FLASH Radiother Int Workshop* (2019) 139:4–10. doi:10.1016/j.radonc.2019.06.006

5. Vozenin MC, De Fornel P, Petersson K, Favaudon V, Jaccard M, Germond JF, et al. The advantage of FLASH radiotherapy confirmed in mini-pig and cat-cancer patients. *Clin Cancer Res* (2019) 25:35–42. doi:10.1158/1078-0432.CCR-17-3375

6. Lin B, Gao F, Yang Y, Wu D, Zhang Y, Feng G, et al. FLASH radiotherapy: history and future. *Front Oncol* (2021) 11:644400. doi:10.3389/fonc.2021.644400

7. Atkinson J, Bezak E, Le H, Kempson I. The current status of FLASH particle therapy: a systematic review. *Phys Eng Sci Med* (2023) 46:529–60. doi:10.1007/s13246-023-01266-z

8. Sarti A, De Maria P, Battistoni G, De Simoni M, Di Felice C, Dong Y, et al. Deep seated tumour treatments with electrons of high energy delivered at FLASH rates: the example of prostate cancer. *Front Oncol* (2021) 11:777852. doi:10.3389/fonc.2021.777852

9. Böhlen TT, Germond JF, Traneus E, Bourhis J, Vozenin MC, Bailat C, et al. Characteristics of very high-energy electron beams for the irradiation of deep-seated targets. *Med Phys* (2021) 48:3958–67. doi:10.1002/mp.14891

10. Giuliano L, Franciosini G, Palumbo L, Aggar L, Dutreix M, Faillace L, et al. Characterization of ultra-high-dose rate electron beams with ElectronFlash linac. *Appl Sci* (2023) 13:631. doi:10.3390/app13010631

11. Lempart M, Blad B, Adrian G, Bäck S, Knöös T, Ceberg C, et al. Modifying a clinical linear accelerator for delivery of ultra-high dose rate irradiation. *Radiother Oncol* (2019) 139:40–5. doi:10.1016/j.radonc.2019.01.031

12. Rahman M, Ashraf MR, Zhang R, Bruza P, Dexter CA, Thompson L, et al. Electron FLASH delivery at treatment room isocenter for efficient reversible conversion of a clinical LINAC. *Int J Radiat Oncol - Biol - Phys* (2021) 110:872–82. doi:10.1016/j.ijrobp.2021.01.011

13. Gonçalves Jorge P, Grilj V, Bourhis J, Vozenin MC, Germond JF, Bochud F, et al. Technical note: validation of an ultrahigh dose rate pulsed electron beam monitoring system using a current transformer for FLASH preclinical studies. *Med Phys* (2022) 49:1831–8. doi:10.1002/mp.15474

14. Jain S, Cetnar A, Woollard J, Gupta N, Blakaj D, Chakravarti A, et al. Pulse parameter optimizer: an efficient tool for achieving prescribed dose and dose rate with electron FLASH platforms. *Phys Med Biol* (2023) 68:19NT01. doi:10.1088/1361-6560/acf63e

15. Vignati A, Giordanengo S, Fausti F, Martì Villarreal OA, Mas Milian F, Mazza G, et al. Beam monitors for tomorrow: the challenges of electron and photon FLASH RT. *Front Phys* (2020) 8. doi:10.3389/fphy.2020.00375

16. Qi ZY, Deng XW, Huang SM, Zhang L, He ZC, Allen Li X, et al. *In vivo* verification of superficial dose for head and neck treatments using intensity-modulated techniques. *Med Phys* (2009) 36:59–70. doi:10.1118/1.3030951

17. McDermott PN. Surface dose and acute skin reactions in external beam breast radiotherapy. *Med Dosimetry* (2020) 45:153–8. doi:10.1016/j.meddos.2019.09.001

18. Valentin J. Basic anatomical and physiological data for use in radiological protection: reference values: ICRP Publication 89: approved by the Commission in September 2001. *Ann ICRP* (2002) 32:1–277. doi:10.1016/S0146-6453(03)00002-2

19. Ronga MG, Cavallone M, Patriarca A, Leite AM, Loap P, Favaudon V, et al. Back to the future: very high-energy electrons (VHEEs) and their potential application in radiation therapy. *Cancers* (2021) 13:4942. doi:10.3390/cancers13194942

20. DesRosiers C, Moskvin V, Bielajew AF, Papiez L. 150-250 MeV electron beams in radiation therapy. *Phys Med Biol* (2000) 45:1781–805. doi:10.1088/0031-9155/45/7/306

21. Papiez L, DesRosiers C, Moskvin V. Very high energy electrons (50-250 MeV) and radiation therapy. *Technol Cancer Res Treat* (2002) 1:105–10. doi:10.1177/153303460200100202

22. Szpala S, Huang V, Zhao Y, Kyle A, Minchinton A, Karan T, et al. Dosimetry with a clinical linac adapted to FLASH electron beams. *J Appl Clin Med Phys* (2021) 22:50–9. doi:10.1002/acm2.13270

23. Jaccard M, Durán MT, Petersson K, Germond JF, Liger P, Vozenin MC, et al. High dose-per-pulse electron beam dosimetry: commissioning of the Oriatron eRT6 prototype linear accelerator for preclinical use. *Med Phys* (2018) 45:863–74. doi:10.1002/mp.12713

24. Gómez F, Gonzalez-Castaño DM, Fernández NG, Pardo-Montero J, Schüller A, Gasparini A, et al. Development of an ultra-thin parallel plate ionization chamber for dosimetry in FLASH radiotherapy. *Med Phys* (2022) 49:4705–14. doi:10.1002/mp.15668

25. Bass GA, Shipley DR, Flynn SF, Thomas RAS. A prototype low-cost secondary standard calorimeter for reference dosimetry with ultra-high pulse dose rates. *Br J Radiol* (2023) 96:20220638. doi:10.1259/bjr.20220638

26. Fleetwood D, Winokur P, Schwank J. Using laboratory X-ray and cobalt-60 irradiations to predict CMOS device response in strategic and space environments. *IEEE Trans Nucl Sci* (1988) 35:1497–505. doi:10.1109/23.25487

27. Kwan I, Rosenfeld A, Qi Z, Wilkinson D, Lerch M, Cutajar D, et al. Skin dosimetry with new MOSFET detectors. *Radiat Measurements* (2008) 43:929–32. doi:10.1016/j.radmeas.2007.12.052

28. Patterson E, Stokes P, Cutajar D, Rosenfeld A, Baines J, Metcalfe P, et al. High-resolution entry and exit surface dosimetry in a 1.5 T MR-linac. *Phys Eng Sci Med* (2023) 46:787–800. doi:10.1007/s13246-023-01251-6

29. Tai M, Patterson E, Metcalfe PE, Rosenfeld A, Oborn BM. Skin dose modeling and measurement in a high field in-line MRI-linac system. *Front Phys* (2022) 10. doi:10.3389/fphy.2022.902744

30. Thorpe NK, Cutajar D, Lian C, Pitney M, Friedman D, Perevertaylo V, et al. A comparison of entrance skin dose delivered by clinical angiographic c-arms using the real-time dosimeter: the MOSkin. *Australas Phys Eng Sci Med* (2016) 39:423–30. doi:10.1007/s13246-016-0435-0

31. Alnawaf H, Butson M, Yu PKN. Measurement and effects of MOSKIN detectors on skin dose during high energy radiotherapy treatment. *Australas Phys Eng Sci Med* (2012) 35:321–8. doi:10.1007/s13246-012-0153-1

32. Souris JS, Cheng SH, Pelizzari C, Chen NT, La Riviere P, Chen CT, et al. Radioluminescence characterization of *in situ* x-ray nanodosimeters: potential real-time monitors and modulators of external beam radiation therapy. *Appl Phys Lett* (2014) 105:203110. doi:10.1063/1.4900962

33. Jornet N, Carrasco P, Jurado D, Ruiz A, Eudaldo T, Ribas M. Comparison study of MOSFET detectors and diodes for entrance *in vivo* dosimetry in 18 MV x-ray beams. *Med Phys* (2004) 31:2534–42. doi:10.1118/1.1785452

34. Fleetwood DM. Perspective on radiation effects in nanoscale metal–oxide–semiconductor devices. *Appl Phys Lett* (2022) 121:070503. doi:10.1063/5.0105173

35. Rosenfeld AB. MOSFET dosimetry on modern radiation oncology modalities. *Radiat Prot Dosimetry* (2002) 101:393–8. doi:10.1093/oxfordjournals.rpd.a006009

36. Qi ZY, Deng XW, Huang SM, Lu J, Lerch M, Cutajar D, et al. Verification of the plan dosimetry for high dose rate brachytherapy using metal–oxide–semiconductor field effect transistor detectors. *Med Phys* (2007) 34:2007–13. doi:10.1118/1.2736288

37. Jong W, Ung N, Tiong A, Rosenfeld A, Wong J. Characterisation of a MOSFET-based detector for dose measurement under megavoltage electron beam radiotherapy. *Radiat Phys Chem* (2018) 144:76–84. doi:10.1016/j.radphyschem.2017.11.021

38. Choi JH, Cutajar D, Metcalfe P, Downes S. Application of MOSkin detector for *in vivo* dosimetry on total skin electron therapy (TSET). *Biomed Phys Eng Express* (2018) 4:024002. doi:10.1088/2057-1976/aaac61

39. Shepard AJ, Matrosic CK, Radtke JL, Jupitz SA, Culberson WS, Bednarz BP. Technical Note: characterization of clinical linear accelerator triggering latency for motion management system development. *Med Phys* (2018) 45:4816–21. doi:10.1002/mp.13191

40. Metcalfe P, Kron T, Hoban P, Cutajar D, Hardcastle N. *The Physics of radiotherapy X-rays and electrons*. 3rd ed. Madison, WI: Medical Physics Publishing (2023).

41. Romano F, Bailat C, Jorge PG, Lerch MLF, Darafsheh A. Ultra-high dose rate dosimetry: challenges and opportunities for FLASH radiation therapy. *Med Phys* (2022) 49:4912–32. doi:10.1002/mp.15649

42. Di Martino F, Barca P, Barone S, Bortoli E, Borgheresi R, De Stefano S, et al. FLASH radiotherapy with electrons: issues related to the production, monitoring, and dosimetric characterization of the beam. *Front Phys* (2020) 8. doi:10.3389/fphy.2020.570697

43. Oldham TR. Ionizing radiation effects in MOS oxides. In: *International series on advances in solid state electronics and technology*. World Scientific (2000). doi:10.1142/3655

44. Jong WL, Wong J, Ung NM, Ng KH, Ho G, Cutajar D, et al. Characterization of MOSkin detector for *in vivo* skin dose measurement during megavoltage radiotherapy. *J Appl Clin Med Phys/Am Coll Med Phys* (2014) 15:120–32. doi:10.1120/jacmp.v15i5.4869

45. Meier E, Dowd R, LeBlanc G. Characterization of the Australian synchrotron linac. *Nucl Instr Methods Phys Res Section A: Acc Spectrometers, Detectors Associated Equipment* (2008) 589:157–66. doi:10.1016/j.nima.2008.02.009

46. Schneider CA, Rasband WS, Eliceiri KW. NIH Image to ImageJ: 25 years of image analysis. *Nat Methods* (2012) 9:671–5. doi:10.1038/nmeth.2089

47. Moffat AFJ. A theoretical investigation of focal stellar images in the photographic emulsion and application to photographic photometry. *Astron Astrophysics* (1969) 3:455.